Article

Immobilization secondary to cell death of muscle precursors with a dual transcriptional signature contributes to the emu wing skeletal pattern

Eriko Tsuboi [1,7], Satomi F. Ono [1,7], Ingrid Rosenburg Cordeiro [1,6,7], Reiko Yu [1], Toru Kawanishi [1], Makoto Koizumi [2], Shuji Shigenobu [3], Guojun Sheng [4], Masataka Okabe [5] & Mikiko Tanaka [1] ✉

Limb reduction has occurred multiple times in tetrapod history. Among ratites, wing reductions range from mild vestigialization to complete loss, with emus (*Dromaius novaehollandiae*) serving as a model for studying the genetic mechanisms behind limb reduction. Here, we explore the developmental mechanisms underlying wing reduction in emu. Our analyses reveal that immobilization resulting from the absence of distal muscles contributes to skeletal shortening, fusion and left-right intraindividual variation. Expression analysis and single cell-RNA sequencing identify muscle progenitors displaying a dual lateral plate mesodermal and myogenic signature. These cells aggregate at the proximal region of wing buds and undergo cell death. We propose that this cell death, linked to the lack of distal muscle masses, underlines the morphological features and variability in skeletal elements due to reduced mechanical loading. Our results demonstrate that differential mobility during embryonic development may drive morphological diversification in vestigial structures.

Limb reduction has occurred multiple times throughout tetrapod evolution. Snakes, legless lizards and caecilians have lost their limbs, cetaceans reduced their hindlimbs, and ungulates evolved a reduced number of digits. The reduction of limbs in tetrapods is associated with the diversification of their locomotion styles and habitats. Therefore, revealing the mechanisms by which limb reduction occurs is one of the main themes of tetrapod limb evolution research[1].

Among birds, the forelimb reductions found in ratites range from the mild vestigialization seen in the ostrich to the complete loss of the

forelimb in the extinct moa, and might have occurred multiple times in this clade[2,3]. Of the ratites available for developmental approaches, the emu exhibits an extreme forelimb reduction, which is already evident during embryonic as a very reduced forelimb bud[4]. Several groups have addressed mechanisms of forelimb bud reduction during early stages of emu limb development, which has been attributed to decreased proliferation of limb bud progenitors, and also to a heterochrony caused by modulation and/or delayed expression of typical limb patterning genes[2,5–10], including higher variability in expression

[1]School of Life Science and Technology, Tokyo Institute of Technology, B-17, 4259 Nagatsuta-cho, Midori-ku, Yokohama, Kanagawa, Japan. [2]Laboratory Animal Facilities, The Jikei University School of Medicine, 3-25-8 Nishi-shimbashi, Minato-ku, Tokyo, Japan. [3]Trans-Omics Facility, National Institute for Basic Biology, Nishigonaka 38, Myodaiji, Okazaki, Aichi, Japan. [4]International Research Center for Medical Sciences, Kumamoto University, 2-2-1 Honjo, Chuo-ku, Kumamoto, Japan. [5]Department of Anatomy, The Jikei University School of Medicine, 3-25-8 Nishi-shimbashi, Minato-ku, Tokyo, Japan. [6]Present address: Department of Cell and Molecular Biology, Karolinska Institutet, Stockholm, Sweden. [7]These authors contributed equally: Eriko Tsuboi, Satomi F. Ono, Ingrid Rosenburg Cordeiro. ✉e-mail: mitanaka@bio.titech.ac.jp

pattern, such as *Grem1*[8]. Nevertheless, a limb bud is formed, which develops into a patterned wing[4].

However, reduction of the actual limb bud does not explain mechanisms taking place during later developmental stages that further shape the emu wings, especially their autopodial region. While three digits are initially specified in the emu autopod[7], most of the cartilaginous elements of the digits 2 and 4 are resorbed during late foetal development[8], which is followed by fusion of skeletal elements and joint contractures that are typical of adult emu wings[8,11]. These appendages display an extensive osteological variation, including presence or absence of phalanges, shape, bone pneumaticity, and muscle attachment[11]. These differences were not restricted to skeletal elements, as it was found that emus lacked several muscle masses in their wings when compared to volant birds as well[11].

Interestingly, defects in both bone growth and joint formation can be secondary to a loss of movement during development, which has been extensively studied in both animal models[12–16] and clinical examples[17]. Limb skeletal defects have been reported in several strains of muscle-less and muscle dysgenesis mice, while avian *in ovo* models have been crucial to pinpoint the effects of early or late immobilization on longitudinal skeletal growth and joint cavitation[13–16,18–30]. In human patients, a decrease in fetal movement can lead to fetal akinesia deformation sequence, a spectrum of skeletal and joint phenotypes[13]. Furthermore, congenital joint contractures often present with a range of severity, including variation in the affected joints and, to a lesser extent, asymmetric presentation—even when the cause of the disease has been mapped to a specific mutation[17]. The highly variable range of phenotypes found in emu wings led us to hypothesize whether it was not only the result of direct genetic factors but also secondary to extrinsic epigenetic factors—more specifically, to a reduced mechanical stimulation.

Here, we show that emu forelimbs exhibit a high intraindividual asymmetry in skeletal patterns, in addition to a reduction in bone length and contractures of joints. Such morphological features seen in emu forelimbs recapitulate the skeletal phenotype found in both experimental and clinical observations of reduced mechanical loading during limb development. In addition, we observe a lack of distal limb movement in emu embryos resulting from the lack of muscle masses at the distal ends of their wings, a condition that is apparent from the stages of prenatal development. Single-cell RNA sequencing (scRNA-seq) data and expression analysis revealed that a subpopulation of muscle progenitors exhibits a dual myogenic/LPM (lateral plate mesoderm) transcriptional signature. This subpopulation undergoes massive cell death and thereby fails to form distal skeletal muscles, which contributes to the unique morphology of emu forelimbs.

Results

High intraindividual left-right variation is found in the adult skeletal pattern of the distal emu wings

Previously, we and others have shown that a great range of interindividual variation exists in the digital pattern of adult emu forelimbs[8,11]. Understanding whether the variation is present within limbs of the same individual, or is consistent between left and right limbs, would help elucidate the source of variation itself. Here, a comparison between the pair of forelimbs of eight adult emu specimens revealed an intraindividual, left–right asymmetric skeletal pattern (Fig. 1a; Supplementary Fig. 1a). The variation included different status regarding fusion of the ulna and radius, fusion of autopodial skeletal elements, fusion of joints and bone pneumaticity between left and right limbs of the same individual (Fig. 1a). Furthermore, the humeral, ulnar and metacarpal lengths were relatively asymmetric in all examined emu forelimbs compared to chicken forelimbs (Fig. 1b; Supplementary Fig. 1b). Thus, there is a high degree of intra- and interindividual variability intrinsic to emu wing skeletal elements.

Developing emu forelimbs receive less mechanical input due to the absence of distal muscle masses

Studies in chicken and mouse embryos revealed that longitudinal bone growth of the limb and normal joint cavity formation require mechanical input as a result of embryonic muscle contraction[13,19–29]. Importantly, a marked reduction in the number of muscle masses is found in adult emu wings, especially towards its distal part[11], although the remaining muscles display a typical skeletal muscle morphology (Supplementary Fig. 1c). A normal gross morphology of the forelimb muscle masses has been reported in stage 30 emu forelimbs[7]; however, it remains unclear when muscle reduction occurs during autopodial development, which takes place at later stages. To address this question, we analyzed the process of muscle formation in developing forelimb buds of emu embryos and compared them to those in chicken embryos (Fig. 1c; Supplementary Fig. 2a). At stage 30, both chicken and emu display the typical avian forelimb structure containing three digits[7]. While no autopodial muscle mass could be detected at this stage (Supplementary Fig. 2a), they became evident at stages 33, 35 and 37 (Fig. 1c; Supplementary Fig. 2a). In contrast, digits 2 and 4 of emu wings displayed various degrees of vestigialization, which takes place up to stage 37[8]. No autopodial muscles were observed, and most zeugopodial muscles were missing from developing emu forelimb buds up to stage 37 (Fig. 1c; Supplementary Fig. 2a). By recording embryonic movement *in ovo*, we also found that the distal part of forelimb buds showed hardly any movement in emu embryos at stage 39, while embryonic muscle contraction was already evident in the distal forelimb buds in chicken embryos or the proximal portion of emu wings at the same stage (Fig. 1d; Supplementary Fig. 2b). These results demonstrate that the distal part of the emu forelimb receives less mechanical input during its development in connection to the absence of distal muscle formation.

Loss of mobility recapitulates characteristic features of emu forelimbs

Much research has been devoted to understanding the effect of muscle contraction on the growth of limb bones and joint cavity formation in avian limbs[13,15,16,24–32]. Although the decreased mechanical load secondary to the absence of distal muscle could explain the left–right variation seen in the emu forelimb skeleton, to our knowledge, there have been no reports demonstrating the effect of immobilization specifically on intraindividual left–right asymmetric patterning of limbs. Here, we will address these questions by first focusing on the effect of late-stage immobilization (E10-18) on the longitudinal growth of individual skeletal elements, followed by examining how immobilization starting at pre-cavitation stages (E6-E10) could affect both growth and joint cavitation asymmetrically.

Firstly, we induced rigid paralysis in chicken embryos under conditions known to lead to a reduction in the length of hindlimbs after joint cavitation occurs[13,24–29] and examined the length of skeletal elements, joint cavity formation and left–right patterning of forelimbs (Supplementary Fig. 3). The lengths of both the right and left humerus, ulna and metacarpus of digit 3 were significantly reduced in chicken embryos immobilized between E10-18 (Supplementary Fig. 3a, b). Pharmacologically induced immobility also led to drastic intraindividual variation in the length of the left and right humerus, ulna and metacarpus, compared to controls (Fig. 1e). These results suggest that mobility is necessary for symmetric limb patterning and growth.

Intriguingly, even upon immobilization at a post cavitation stage, two out of thirteen immobilized chickens showed an asymmetric pattern at the wrist joint with fusion of cartilaginous fusion of limb elements (Supplementary Fig. 3c). To understand further the effect of mechanical inputs on symmetrical growth and patterning of autopodial skeletal elements, we have immobilized chicken embryos from E6 (Supplementary Figs. 3d, 5 and 6), when muscle masses had
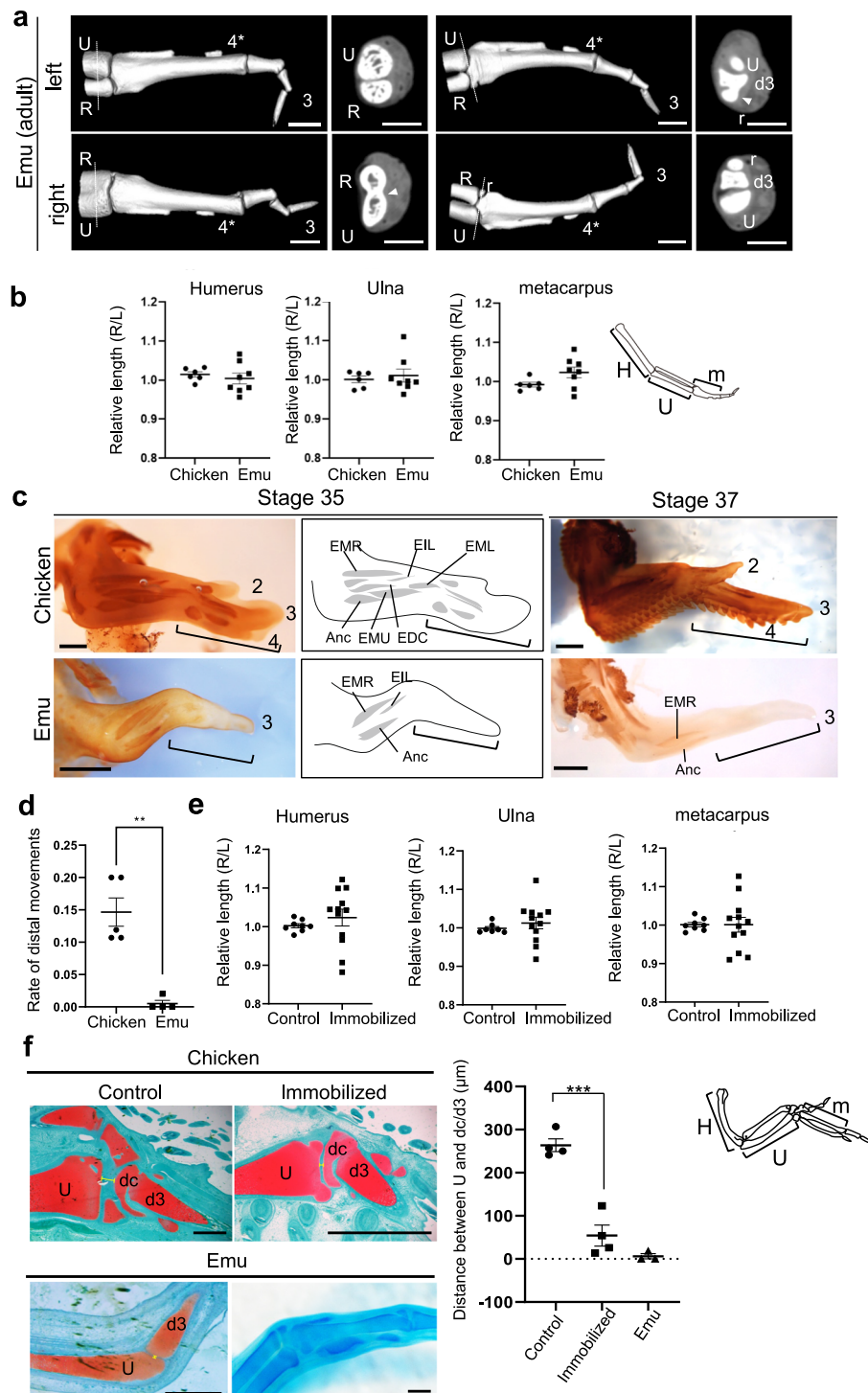
developed, and forelimb movements were apparent (Supplementary Fig. 4a, b). The total length of skeletal elements of digits (metacarpus and phalanges) was significantly reduced compared to that in controls for all digits (Supplementary Fig. 5b). In addition, the reduction in digit length was relatively asymmetric in digits 2 and 4, while the reduction in digit 3 was relatively symmetric (Supplementary Fig. 5c). Of note, emu forelimbs exhibit severe reduction of digits 2 and 4 as well, but not of digit 3 (Fig. 1a; Supplementary Fig. 1a).

As previously described[12], immobilization of the chicken embryo at pre-cavitation stages led to a failure of proper joint cavity formation at the wrist region; we have observed that the cartilaginous fusion of

skeletal elements was also asymmetric (Fig. 1f; Supplementary Fig. 6). Thinning or absence of the joint cavity at the wrist is one of the characteristic features of the emu forelimb skeletal pattern[8] (Fig. 1a). Immobilization significantly reduced the distance between the ulna and the distal carpal in chicken embryos (Fig. 1f). Similar to immobilized chickens, the distance between the ulna and the metacarpus of digit 3 was also narrow in emu embryos at the same stage of development (Fig. 1f). These results indicate that loss of mobility from early stages recapitulated characteristic features of emu forelimbs, such as reduction or loss of the joint cavity at the wrist caused by asymmetric fusion of skeletal elements.

Fig. 1 | Skeletal and muscular patterns of the forelimb of emu and chicken.
a Three-dimensional renderings from CT images of the distal part of adult emu
forelimb skeletons and transverse sections taken from the emu limb at the level of
the dashed line. The left and right limbs of two specimens are shown. Arrowheads
indicate the fusions. 3-4, digits 3-4; 4*, rudiment of digit 4; d3, metacarpal of digit 3;
r, radiale; R, Radius; U, ulna. Scale bars, 1 cm. **b** Ratio of left to right bone length
(coefficient of variation: 2.23%, 3.60 %, 1.93%, 4.24%, 0.59%, 3.54% for chicken
humerus, emu humerus, chicken ulna, emu ulna, chicken metacarpus, emu meta-
carpus, respectively). Mean ± SEM. $n = 6$ (chicken), $n = 8$ (emu). **c** Immunostaining
with MF20 in forelimbs of chicken and emu embryos. Although the formation of
muscles was recognized in autopodial regions of stage 35 ($n = 4$) and 37 ($n = 5$)
chicken embryos, no autopodial muscles and only a few or no zeugopodial muscles
were observed in the forelimbs of emu embryos at the same stages (EMR, EIL, Anc
on the dorsal side and the flexor carpi ulnaris (FCU) on the ventral side at stage 35
($n = 3$); EMR, Anc on the dorsal side and FCU on the ventral side ($n = 1$), Anc only
($n = 1$), no muscles ($n = 1$)). Brackets indicate autopodial regions. 2-4, digits 2-4; Anc,

anconeus; EDC, extensor digitorum communis; EIL, extensor indicis longus; EML,
extensor medius longus; EMR, extensor metacarpi radialis. Scale bars, 1 mm. **d** Rate
of distal movements (see Materials and Methods for details). $n = 5$ (chicken), $n = 4$
(emu). Mean ± SEM. Welch's two tailed t-test. **$p = 0.0023$. **e** Ratio of left to right
bone length of chicken embryos treated with PBS ($n = 7$) or DMB (n = 13) from E10 to
E18 (coefficient of variation: 1.39%, 7.08%, 1.17%, 4.66%, 1.37%, 5.93% for control
humerus, immobilized humerus, control ulna, immobilized ulna, control meta-
carpus, immobilized metacarpus, respectively). **f** Chicken embryos were treated
with PBS or DMB from E6 (stage 28) to E14 (stage 39). Safranin O staining of the
wrist joints of chicken and emu embryos and Alcian blue staining of forelimbs of
emu embryos. The control panel is flipped horizontally. The distance between the
ulna and the distal carpal/metacarpal of digit 3 (yellow lines) was measured in
control chickens ($n = 4$), immobilized chickens ($n = 4$) and emu embryos ($n = 3$).
Mean ± SEM. Welch's two tailed t-test. ***$p = 0.0003$. dc, distal carpal; d3, meta-
carpal of digit 3; U, ulna. Scale bars, 500 μm.

Taken together, these results reveal that the lack of distal muscle
formation in emu embryos, when compared to chicken, led to a non-
experimental immobilization phenotype that closely resembles
experimental immobilization phenotypes in chicken. Specifically, we
have shown that the reduction in bone length, increased susceptibility
of the digits 2 and 4 to growth reduction when compared to digit 3,
joint fusion and/or joint cavitation defects had an intraindividual
asymmetric presentation in both emu and immobilized chicken
forelimbs.

A population with dual myogenic and LPM cell signature is recognized in emu wings

Our findings suggest that the lack of distal muscle masses in com-
parison with chicken recapitulated, at least partially, the distinctive
skeletal pattern of the emu wing. However, the underlying develop-
mental reasons for the reduction of muscle in emu forelimbs are still
not clear. To explore this, we first studied in detail the developmental
process of forelimb muscles in emu embryos. In amniotes, muscle
precursors delaminated from the ventral dermomyotome extensively
migrate toward the distal part of the limb bud and differentiate into
skeletal muscles. The delamination of muscle precursors in emu takes
place in stages equivalent to chicken[9]; however, they migrate in a dif-
fuse pattern and are not divided into dorsal and ventral muscle masses
when compared to the emu hindlimb[6] or to chicken forelimbs[33]. The
migratory muscle precursors[33] are characterized by the expression of
Lbx1, which encodes a ladybird homeobox transcription factor[34],
thought to be involved in controlling their migration[35–38]. *cMet*, which
encodes a tyrosine kinase receptor, is expressed in the ventral der-
momyotome as well as in muscle precursors migrating toward limb
buds[39–41]. In addition, it has been previously reported that the emu
forelimb bud co-opted *Nkx2.5* expression[7], and *Nkx2.5*-positive cells
become skeletal muscle in forelimbs[7,9]. Thus, we examined the
expression pattern of *Lbx1*, *cMet* as well as *Nkx2.5* in developing emu
wing buds (Fig. 2; Supplementary Figs. 7 and 8). In chickens, the
invasion of *Lbx1*-positive migratory muscle precursors into the fore-
limb bud became apparent at stage 18[33] (Supplementary Fig. 7a). In
emu, transcripts of *Lbx1* and *cMet* were enriched in the lateral region of
the dermomyotome, and their distribution in the forelimb field
became detectable at stage 18 (Fig. 2a). The expression of *Nkx2.5* was
seen only in the anterior edge of the forelimb field at the same stages
(Fig. 2a). By stage 19, *Lbx1/cMet*-positive migratory muscle precursors
invaded into the dorsal one half to one-third of the forelimb bud
region, and *Nkx2.5* expression was observed to the central region of
the anterior three-quarters of limb buds (Fig. 2a, b). At stage 22,
expression of *Nkx2.5* was seen from the cervical to the forelimb level in
the lateral plate mesoderm (Supplementary Fig. 7b). By stage 23, *cMet*
expression was observed in migratory muscle precursors spread
throughout the limb buds, and *Nkx2.5* expression was seen in the

ventral two-thirds of the forelimb bud (Fig. 2b). To observe gene
expression in more detail, in situ hybridization using RNAscope
probes was also used. It was found that *cMet* transcripts were spar-
sely distributed in proximal muscle precursors derived from the
dermomyotome and were more densely distributed in the medial
part of forelimb buds, where *Nkx2.5* transcripts were observed, at
stages 19 and 23 (Fig. 2c; Supplementary Fig. 8). At stage 25, the
expression of *Lbx1* and *Nkx2.5* was observed in the proximal region
and the subapical region, and the expression of *MyoD*, a key reg-
ulator of myogenic differentiation, overlapped with these cells at the
subapical region (Fig. 2b). Co-localization of *cMet* and *Nkx2.5* tran-
scripts were confirmed by using RNAscope probes, and *MyoD* tran-
scripts also co-localized at the subapical region (Fig. 2d;
Supplementary Fig. 8). Subsequently, the expression of *Nkx2.5* was
detected in the skeletal muscles (Supplementary Fig. 7c), as pre-
viously reported[7,9]. Our results and the results of others indicate that
muscle progenitors of emu wings are positive for both *Lbx1* and *cMet*,
marker genes for somite-derived myogenic cells, as well as for
Nkx2.5, a gene typically expressed in the vertebrate cardiac
mesoderm[42].

While skeletal muscle cells and limb bud cells are derived from the
paraxial mesoderm and the somatic layer of the lateral plate meso-
derm (LPM), respectively, the cardiac mesoderm is derived from the
splanchnic layer of the LPM. Thus, these results raised the possibility
that the emu muscle progenitors possess atypical markers, including
ones typically linked to the LPM identity. To investigate gene expres-
sion in an unbiased manner and at single cell resolution, we performed
single-cell RNA sequencing (scRNA-seq) using the Chromium platform
and paired-end Illumina next-generation sequencing of the dissociated
cells from the emu trunk tissue at the forelimb level at stage 20/21 and
the forelimb bud at stage 25. Cells obtained from stage 20/21 trunk
tissues ($n = 2696$) and stage 25 forelimb buds ($n = 7363$) were used for
analyses after quality control of datasets using the Seurat package to
remove potential doublets and low-quality reads. Multidimensional
reduction through tSNE clustering led to the unbiased identification of
the muscle clusters, which contained cells enriched for markers of the
somite-derived myogenic cells, such as *Pax3*[43], *cMet*, and *Lbx1* as well as
markers of skeletal muscle progenitors, such as *TnnT3* (*Troponin T3,
Fast Skeletal Type*), *MyoD1* and *Myog* (*myogenin*) from stages 20/21
trunk tissues at the forelimb level (Fig. 3a, b; Supplementary
Figs. 9 and 10; Supplementary Data 1). Interestingly, in this muscle
cluster, 6.2% of cells expressing both *Pax3* and *Hand2*, which is a
general marker of the lateral plate mesodermal cells[44–47], were identi-
fied (21/339 cells; Fig. 3c). We also identified the muscle clusters
expressing the myogenic markers from stage 25 forelimb buds
(Fig. 3d, e; Supplementary Fig. 11; Supplementary Data 2). In the muscle
cluster of the stage 25 forelimb buds (Fig. 3d, e), 19.2% of muscle
progenitors positive for both *Pax3* and *Hand2* were identified (97/505
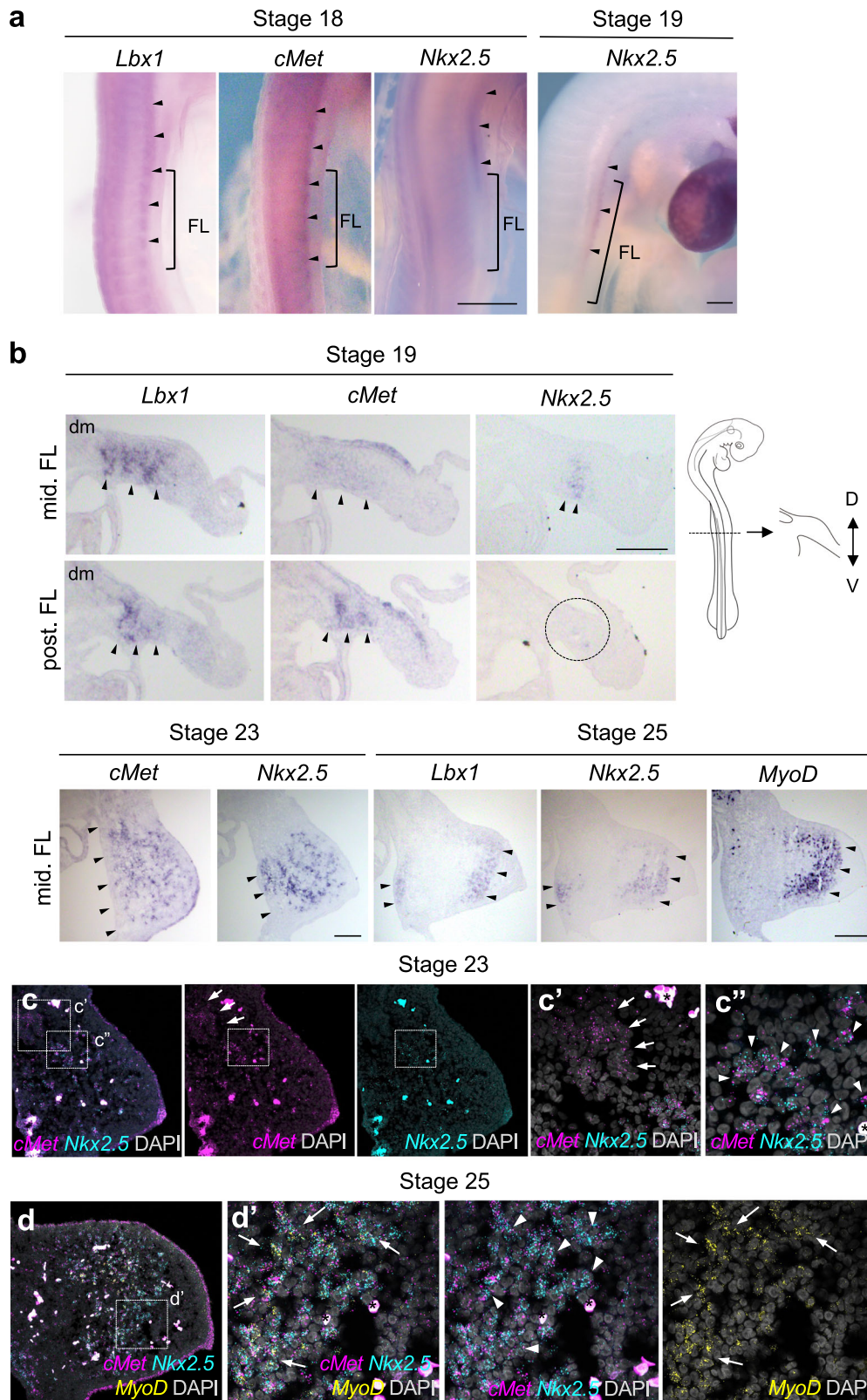
Fig. 2 | Expression of Lbx1, cMet, Nkx2.5 and MyoD in developing emu forelimb buds. a Expression of *Lbx1*, *cMet* and *Nkx2.5* (arrowheads) in forelimb fields (FL) of emu embryos (stage 18 *Lbx1* (*n* = 6), *cMet* (*n* = 2), *Nkx2.5* (*n* = 4); stage 19 *Nkx2.5* (*n* = 2)). Scale bars, 500 μm. **b** Expression of *Lbx1*, *cMet*, *Nkx2.5* and *MyoD* (arrowheads) in serial sections of emu forelimb buds at mid- (mid. FL) or posterior level (post. FL). A dotted circle indicates *Nkx2.5* negative region. Panels of stages 19 and 23 sections were flipped horizontally. (stage 19 *Lbx1* (*n* = 6), *cMet* (*n* = 4), *Nkx2.5* (*n* = 6); stage 23 *cMet* (*n* = 2), *Nkx2.5* (*n* = 2); stage 25 *Lbx1* (*n* = 3), *Nkx2.5* (*n* = 3),

MyoD (*n* = 2)). dm, dermomyotome; D, dorsal; V, ventral. Scale bars, 50 μm. **c, c', c''** Distribution of *cMet* and *Nkx2.5* transcripts in developing emu forelimb buds at stage 23 (*n* = 4). Arrows indicate the *cMet* transcripts in muscle precursors derived from the dermomyotome. Arrowheads indicate co-localized transcripts of *cMet* and *Nkx2.5*. **d, d'** Distribution of *cMet*, *Nkx2.5* and *MyoD* transcripts in emu forelimb buds at stage 25 (*n* = 3). Note that transcripts of *cMet* and *Nkx2.5* (arrowheads) are present in cell clusters, in which *MyoD* expression is also detected (arrows). White cells are blood cells (asterisks), not stained cells.
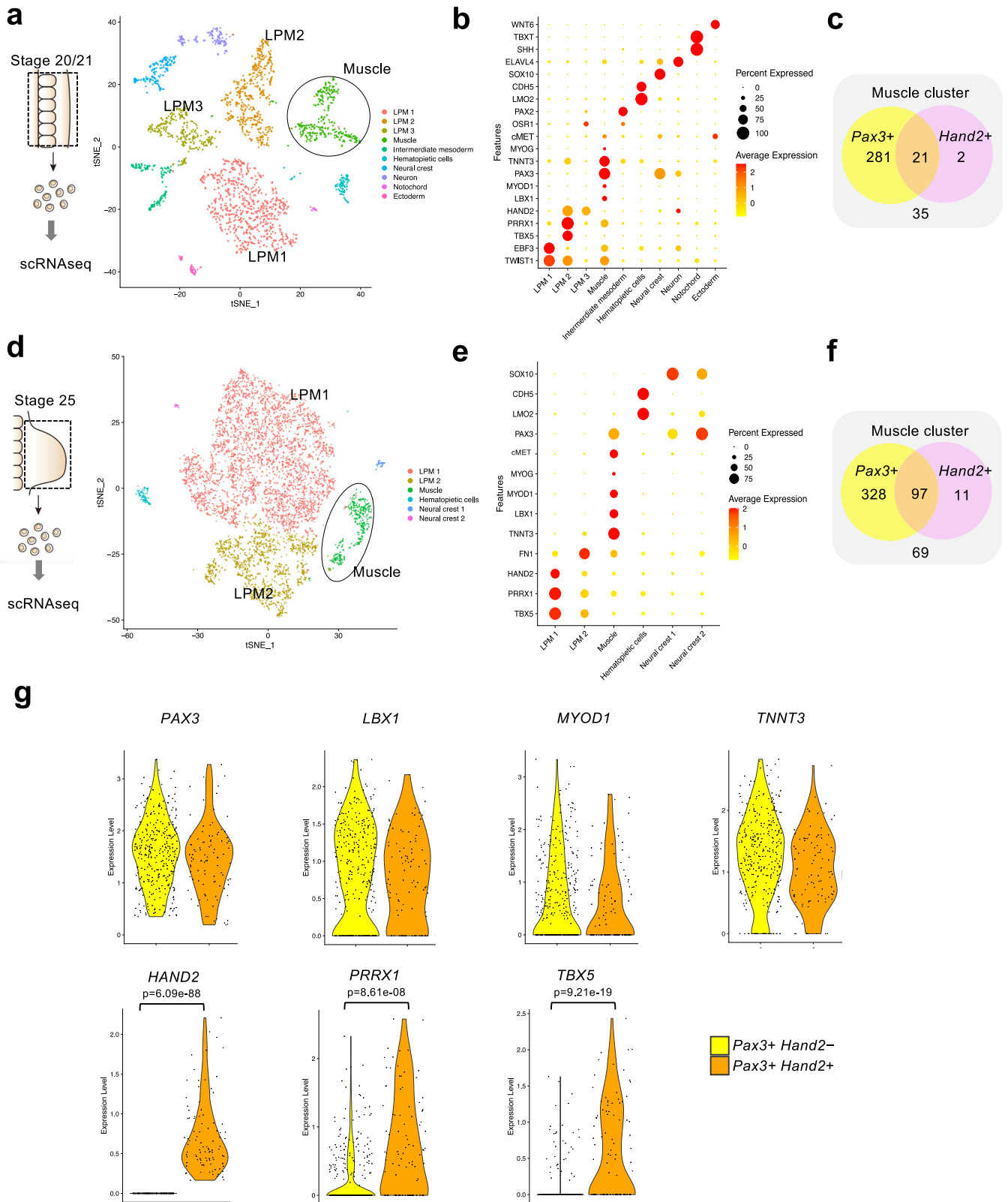
Fig. 3 | A subpopulation of muscle progenitors exhibits a dual somite-derived myogenic cell/LPM cell signature in emu forelimb buds. a, d, tSNE plots of body trunk at the forelimb level of stage 20/21 emu embryo data (a) and stage 25 emu forelimb buds (d), respectively. **b, e,** Dot plots of subcluster marker gene expression of stage 20/21 data (b) and stage 25 data (e), respectively. Dot color represents the average expression level, and dot size represents the percentage of cells expressing marker genes. **c, f,** Venn diagram showing number of cells expressing *Pax3* and/or *Hand2* in the muscle cluster of stage 20/21 data (c) and stage 25 data (f), respectively. **g,** Violin plots showing the expression levels of *Pax3, Lbx1, MyoD1, Tnnt3, Hand2, Prrx1,* and *Tbx5* in *Pax3 + /Hand2-* cells, and *Pax3 + /Hand2+* cells in the muscle cluster of stage 25 emu forelimb data. The two-sided Wilcoxon rank sum-test was used for statistical test. The exact *p*-values are indicated.

cells; Fig. 3f). In this *Pax3+/Hand2+* subpopulation of cells, significantly higher levels of expressions of other somatic LPM cell markers, such as *Prrx1* and *Tbx5*[48–53], compared to the *Pax3+/Hand2-* progenitors were detected (Fig. 3g; Supplementary Data 3). In addition, the expression of *MyoD1* and *Tnnt3* was detected in this *Pax3+/Hand2+* subpopulation (Fig. 3g). These results suggest that the *Pax3+/Hand2+* cells found during emu limb development have a dual transcriptional signature of the somite-derived myogenic cell and the LPM cell.

To determine whether such subpopulation of muscle cells with a dual transcriptional signature is a unique feature of emu forelimbs, we analyzed a publicly available single-cell RNA-seq dataset obtained from stage 24 and 27 chicken forelimb buds[54] and compared them with data from stage 25 emu forelimb buds. In stage 25 emu forelimb buds, we identified clusters of muscle cells enriched with LPM cell markers (Supplementary Fig. 12). In contrast, in stage 24 and 27 chicken forelimb buds, *Hand2* expression was not observed in the extracted cluster of muscle cells, and the expression of other LPM markers were not enriched (Supplementary Fig. 13; Supplementary Data 4-5). This suggests that muscle progenitors with an LPM transcriptional signature are distinctive to emu forelimb buds.

Next, we used in situ hybridization chain reaction (HCR) technique to examine the distribution of the subpopulation of cells with the dual *Pax3+/Hand2+* identity in developing emu forelimb buds (Fig. 4; Supplementary Fig. 14). At stage 19, transcripts of *Pax3* were detected in the dermomyotome and those of *Hand2* were detected in the forelimb mesoderm (Fig. 4a; Supplementary Fig. 14a), but co-localization of *Pax3* and *Hand2* transcripts was not identified in the forelimb buds. By stage 23, although a few cells begin to exhibit a dual transcriptional signature, most *Pax3+* somite-derived myogenic cells and *Hand2+* forelimb mesenchyme can be distinguished from each other (Fig. 4b; Supplementary Fig. 14b). However, by stage 25, *Pax3* transcripts were co-localized with *Hand2* transcripts in a population of cells aggregated at the proximal region of forelimb buds (Fig. 4c, d; Supplementary Fig. 14c, d), and continued to be observed at the same region until stage 27 (Supplementary Fig. 15). This cell population contained extensive pyknotic nuclei when compared with the surrounding cells (Fig. 4c', e; Supplementary Fig. 15). In contrast, in developing chicken forelimb buds, *Pax3+* dermomyotome and muscle progenitors were clearly distinguishable from *Hand2+* mesenchymal cells, and unlike in emu forelimb buds, cell aggregation was not observed in proximal region (Fig. 4f–h; Supplementary Fig. 16). The cell population with pyknotic nuclear feature in emu limb buds appeared to be entrapped at the proximal region by forming aggregates, and most importantly, some of their nuclei were condensed or fragmented (Fig. 4c, d; Supplementary Fig. 15). At this stage, MF20-positive muscle cells were recognized among *Pax3+* migrating muscle progenitors; however, such a strong MF20 staining was either absent or only sparsely recognized in the aggregated cells (Fig. 4d, Supplementary Figs. 14c and 15). Taken together, in emu forelimb buds, a subpopulation of muscle progenitors exhibits a dual *Pax3+* somite-derived myogenic cell/*Hand2+* LPM cell signature and can be located forming aggregates at the proximal region during emu wing development.

A population of muscle progenitors with dual LPM/myogenic cell underwent cell death during wing development

Fragmentation of nuclei seen in the *Pax3+/Hand2+* cell population is a characteristic feature of apoptotic cells. In accordance with this prediction, scRNA-seq data showed that the expression of *BCL2 Antagonist/Killer 1* (*BAK1*), encoding a pro-apoptotic protein, *Caspase-10* (*CASP10*), encoding a cysteine peptidase responsible for the activation of the apoptotic cascade, and *Apoptotic Peptidase Activating Factor 1* (*APAF1*), encoding a cytoplasmic protein that assembles into the apoptosome upon cytochrome c binding, were recognized in the

Pax3+/Hand2+ cell population, albeit not statistically upregulated at expression level (Fig. 5a; Supplementary Data 3). Of note, most cells actively undergoing apoptosis have been eliminated from our scRNA-seq during cell preparation steps (density gradient centrifugation excludes apoptotic bodies) or bioinformatics quality control (exclusion of cells with mtDNA content > 15%). Nevertheless, it remained unclear whether the cells exhibiting nuclear fragmentation were congruent with those identified through scRNA-seq analysis. Therefore, to investigate this further, apoptosis assays were conducted using TUNEL staining, along with immunostaining for cleaved caspase-3 and the oxidative damage marker 8-oxoguanine, on sections of emu forelimb buds (Fig. 5b–d; Supplementary Fig. 17). In this population, cells positive for TUNEL, caspase-3, and 8-oxoguanine were highly abundant (Fig. 5b–d). Additionally, some TUNEL-positive cells in the proximal region were surrounded by MF20-positive cells (Supplementary Fig. 17), suggesting that these dying cells were among muscle progenitors. These findings indicate that a distinct population of muscle progenitor cells, characterized by a dual LPM/myogenic cell signature, undergoes cell death.

Discussion

Here, we show that emu forelimbs exhibit left–right asymmetric skeletal patterns, in addition to a reduction in longitudinal bone growth in the limbs and contractures of wrist joints. The observed morphological traits in emu forelimbs can be attributed to a reduction of mechanical loading from embryonic movements, which in turn is due to the absence of muscles at the distal parts of their forelimbs. Impaired skeletal muscles of emu forelimbs are, at least partially, attributed to massive cell death of a population of muscle progenitors exhibiting a dual LPM/myogenic cell signature.

During myogenesis, muscle progenitors/myoblasts take one of three distinct fates[55]. While the majority of myoblasts fuse to form multinucleated muscle fibers/myotubes, there is a second population of cells located between the basal membrane and the sarcolemma of the muscle fibers that becomes myogenic stem cells/satellite cells. Furthermore, a third population of muscle progenitors that fails to differentiate into muscle fibers undergo programmed cell death[55]. In emu forelimb buds, some of *Pax3+/Hand2-* migrating muscle progenitors expressed high levels of myosin heavy chain (MF20), indicating differentiation into muscle fibers. On the other hand, MF20 signals were hardly detectable in a subpopulation of cells exhibiting a dual LPM/myogenic cell signature, suggesting that these cells might have failed to differentiate into muscle fibers and undergo other 'default' states, such as cell death. It is reasonable to assume that muscle progenitors with a LPM transcriptional signature may not be able to form muscle fibers which usually form by a fusion of cells in a homogenous population of myoblasts. Interestingly, the differentiation of myoblasts into muscle fibers requires activation of caspase-3[56], as well as cytochrome c and Apaf-1[57], suggesting that the mitochondrial death pathway can promote cell fusion as well as cell death. Caspase-dependent non-lethal differentiation has been reported not only in myoblasts, but in a variety of cell types[58,59], however, the mechanisms of how some cell types avoid cell death under the presence of caspase is largely unknown[57]. The duration and intensity of caspase-3/7 activity is shown to be critical to determine whether mouse embryonic stem cells differentiate into cardiomyocytes or undergo cell death[60]. In emu forelimb buds, a subpopulation of cells exhibiting a dual LPM/myogenic cell signature displayed a strong activity of caspase-3, along with oxidative damages of DNA and fragmented nuclei, suggesting caspase-dependent apoptosis occurred. Given that caspase-dependent apoptotic signals are required for differentiation of myoblast into muscle fibers, it is conceivable that cells with a dual LPM/myogenic cell signature fail to differentiate into muscle fibers due to excess level of caspase activity for differentiation, and consequentially, underwent cell death before migrating toward the distal region.
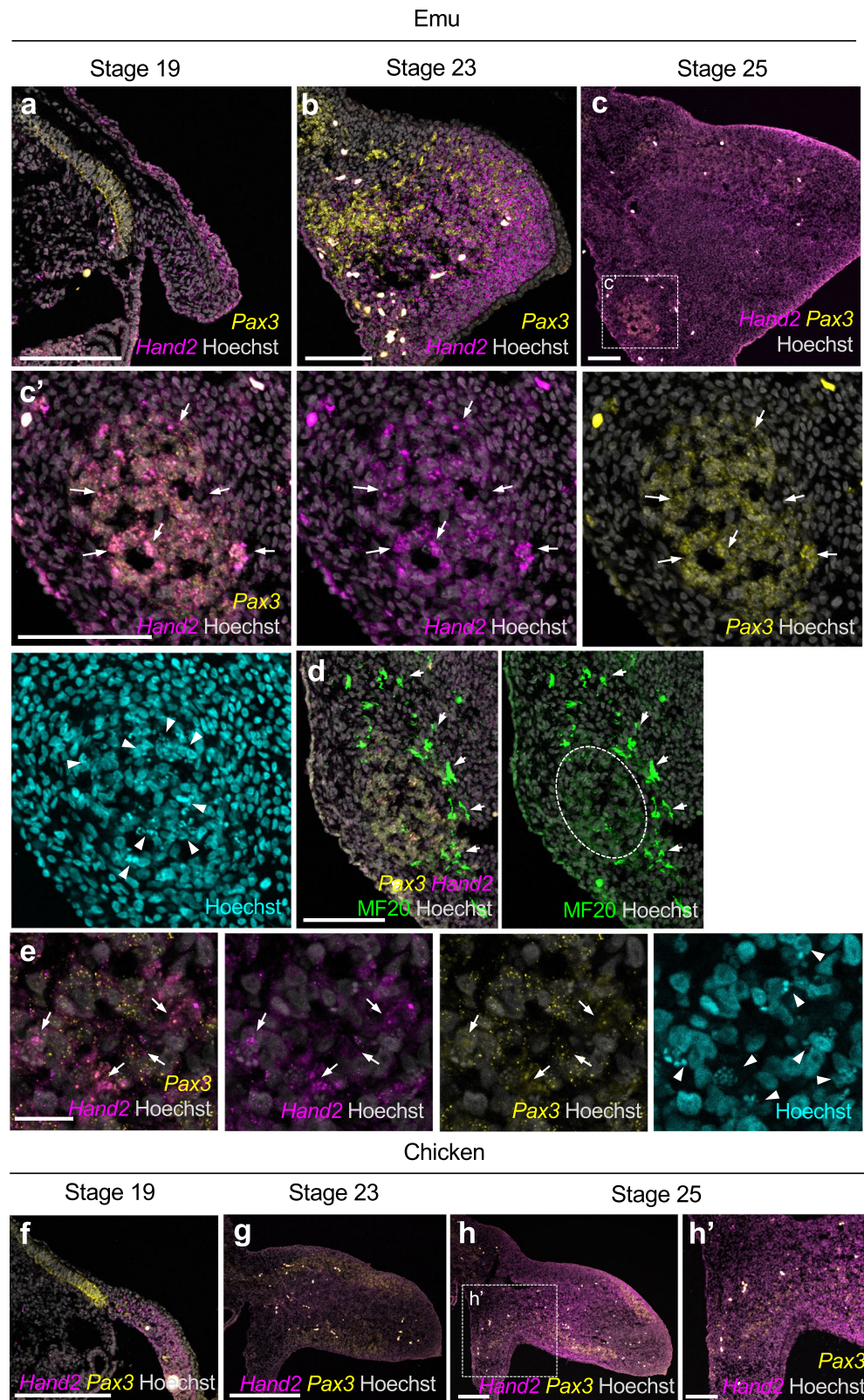
Fig. 4 | A subpopulation of muscle progenitors co-expressing Pax3 and Hand2 aggregates at the proximal region of emu forelimb buds. a–e HCR for *Pax3* and *Hand2* and immunostaining for MF20 in emu forelimb buds at stages 19 (**a**, $n = 2$), 23 (**b**, $n = 3$) and 25 (**c–e**, $n = 3$). **c'** Enlarged images indicated in (**c**). Arrowheads indicate fragmented nuclei. Note that transcripts of both *Pax3* and *Hand2* were observed in aggregated cells (arrows). **d**, Note that MF20 signals (arrows) were not detected in the aggregated cell population (a dotted circle). **e** HCR for *Pax3* and *Hand2* in the aggregated cell population at the proximal region of stage 25 emu

forelimb buds (arrows). Note that transcripts of *Pax3* and *Hand2* are co-localized. Arrowheads indicate fragmented nuclei. **f–h** HCR for *Pax3* and *Hand2* in chicken forelimb buds at stages 19 (**f**, $n = 3$), 23 (**g**, $n = 4$) and 25 (**h**, $n = 2$). **h'** Enlarged images indicated in (**h**). Unlike emu forelimb buds, no aggregated muscle progenitors are observed at the proximal part of chicken forelimb buds at stages 23 or 25. Scale bars, 100 μm (**a–d**, **c'**, **h'**), 20 μm (**e**), 200 μm (**f–h**). Panels of (**a**), (**c**, **c'**) and (**g**) are flipped horizontally.

a *BAK1* *CASP10* *APAF1*

Legend:
- Yellow: *Pax3+ Hand2−*
- Orange: *Pax3+ Hand2+*

b / **b'** TUNEL

c / **c'** Active-caspase-3, Hoechst

d / **d'** 8-oxoguanine, Hoechst

e Stage 19 → Stage 23 → Stage 25

Migratory muscle precursors

Pax3+/*Hand2+* muscle precursors → Cell death

Massive reduction of muscles / No muscle contraction → Asymmetric reduction/fusion of distal skeletal elements
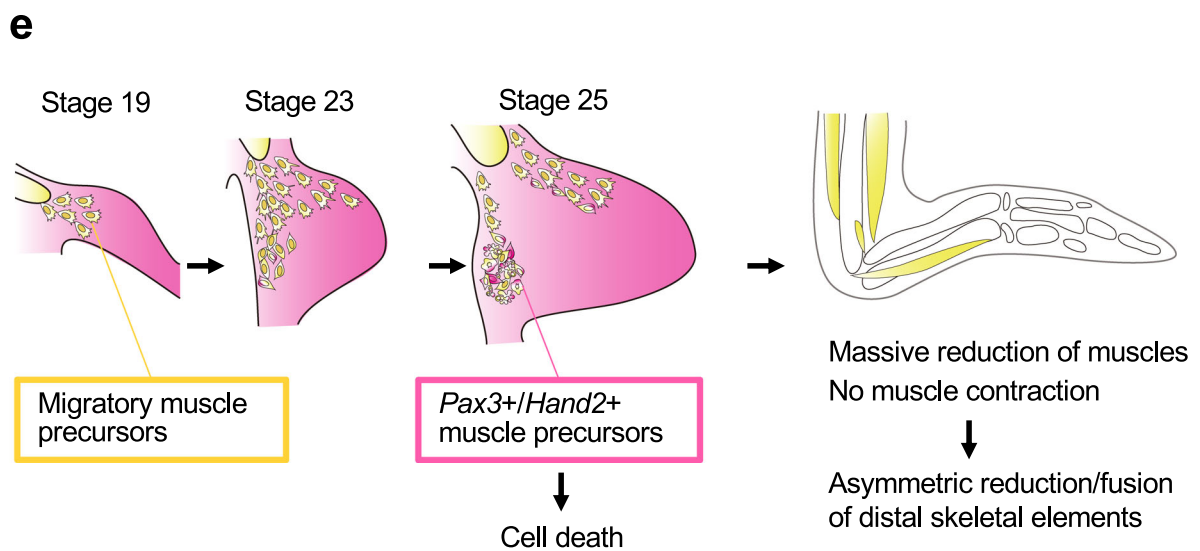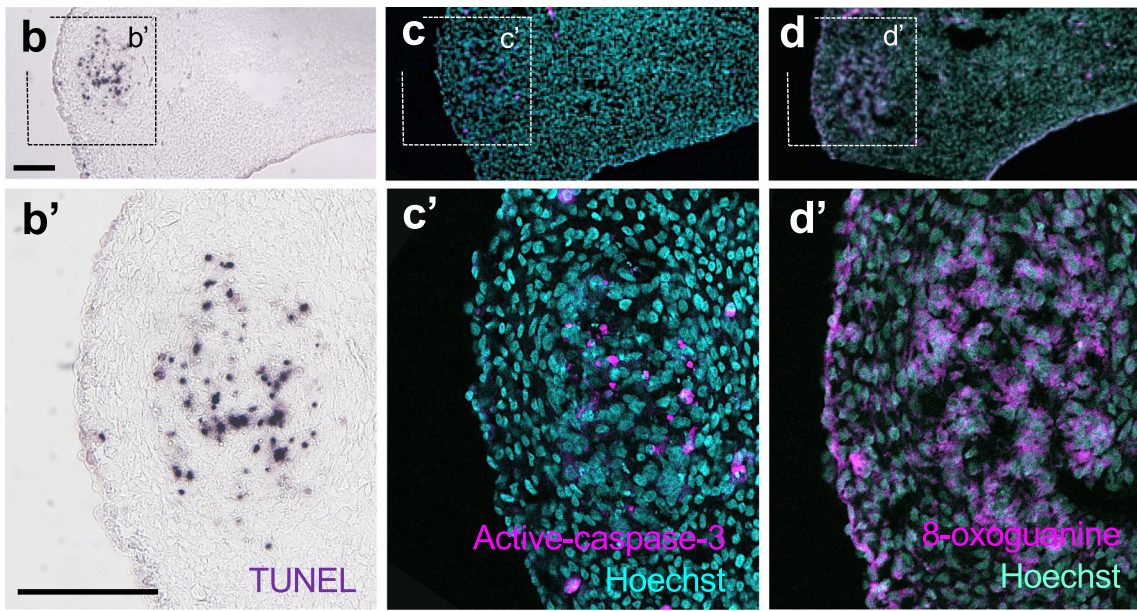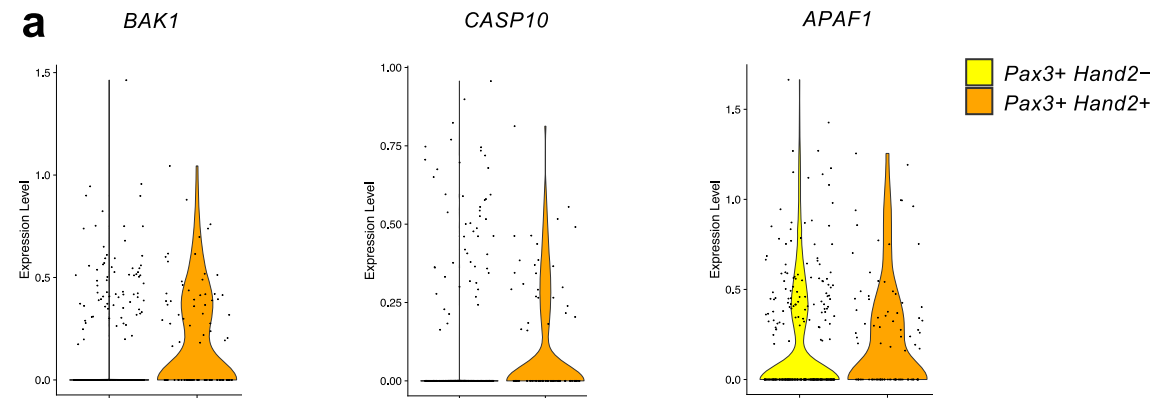
Multiple factors have been associated with the morphological features of emu forelimbs. In the early limb bud of emu embryos, the width of *Grem1* expression domain, which indicates the amount of digit progenitors regulated by the SHH/GREM1/AER-FGF system[61–65], exhibits individual variation[8]. Recent work showed that regulatory changes lead to the lower expression of *Fgf10* and a concomitant failure to express genes related to cell proliferation in the early emu forelimb[9]. Such alterations in gene expression, including a reduction in *Fgf8* expression in the apical ectodermal ridge, might contribute to the individual variation in *Grem1* expression seen in the early limb bud. The reduction in limb proliferation due to the lower expression of *Fgf10* can explain the heterochrony observed in emu forelimb

Fig. 5 | A subpopulation of muscle progenitors aggregated at the proximal region of emu forelimb buds undergoes cell death. a Violin plots showing the expression levels of *Bak1*, *Casp10* and *Apaf1* in *Pax3+/Hand2-* cells, or *Pax3+/Hand2+* cells in the muscle cluster of stage 25 emu forelimb data. **b–d** TUNEL staining (**b**, n = 3), immunostaining for active caspase-3 (**c**, n = 2) and immunostaining for 8-oxoguanine (**d**, n = 2) in the aggregated cell population at the proximal region of stage 25 emu forelimb buds. **b′–d′** Enlarged images indicated in (**b–d**). Panels of (**b, b′**) and (**c, c′**) are flipped horizontally. Scale bars, 50 µm. **e** Schematic model of forelimb development in emu embryos. Migratory muscle precursors (*Pax3+, Lbx1+, cMet+*)

delaminated from the ventral edge of the dermomyotome and begin to migrate into the forelimb mesenchyme (*Hand2+, Prrx1+, Tbx5+*). Subsequently, a subpopulation of muscle precursors with a dual somite-derived myogenic cell (*Pax3+, Lbx1+, cMet+*) /LPM cell (*Hand2+, Prrx1+, Tbx5+*) appears and aggregates at the proximal part of forelimb buds. This aggregated cell population undergoes cell death and thereby failing to form majority of muscles. Impaired formation of limb muscles seems to be at least partially responsible for the asymmetric reduction or fusion of distal skeletal elements. Our results and those of others[2,5–9] suggest that multiple mechanisms contribute to the unique emu wing morphology. See text for details.

outgrowth[6,9]. Loss of embryonic mobility also resulted in a late-stage reduction in the forelimb growth (Fig. 2b), as previously shown for hindlimbs of both chicken and crocodiles[29]. Thus, the lack of movement of the distal part of the forelimb might also be a source of the heterochronic development found at later stages in emu forelimbs[6] in regard to their skeletal development. Massive cell death of muscle progenitors is correlated with the reduction of muscle masses in the emu forelimb, which became evident at later stages (Fig. 1c) as well as in adult wings[11]. The resulting decrease in mechanical stimulation, essential for osteoblast differentiation[66], likely results in a scarcity of specified skeletal progenitors. This scarcity contributes to a range of skeletal alteration, such as the reduction and fusion of skeletal elements, reflecting the skeletal abnormalities observed subsequent to the loss of mobility during embryonic and fetal stages[12]. These data suggest an integrated model in which multiple mechanisms contribute to the extreme reduction and unique phenotype of the flightless emu wing.

We propose that the morphological features seen in emu forelimbs are, at least partially, attributed to a reduction in mechanical loading from embryonic movements, which is caused by the absence of distal muscles. Impaired development of forelimb muscles seems to be associated with the massive cell death of muscle progenitors with a dual LPM/myogenic cell signature. These progenitor cells accumulate at the proximal region, thereby losing their motility, and eventually undergoes cell death (Fig. 5e).

Mechanical loading from embryonic movements, which can be influenced by a range of environmental factors, has been suggested to contribute to the establishment of various skeletal design of limbs[13,15,16,29,31]. The locomotory system displays a remarkable integration between its muscular and skeletal components, allowing for coordinated phenotypic changes throughout evolution. The interdependency of these systems can be identified at several organizational levels. For example, at a molecular level, the mechanotransducer and transcriptional regulator YAP regulates the development of both the skeleton[67,68] and muscle[69]. At a cellular level, cells with dual muscle and LPM identity were identified during mouse limb development and play an important role in integrating the skeletal and muscle compartments at the myotendinous junctions[69–71]. And finally, at organismal level, the "two-legged goat" example reveals how a change in behavior led to morphological traits that phenocopied several evolutionary novelties found in bipedal mammals, in a remarkable example of plasticity that is only possible when the development of muscular and skeletal compartments is strongly coordinated[72].

Species-specific traits can arise not only from distinct load bearing on the adult skeleton, but also from differential motility affecting skeletal proportions and joint formation during development[31]. In a contrasting example of morphological evolution driven by a naturally occurring immobilization, the intrinsic muscles of jerboa feet disappear by a muscle atrophy mechanism without evidence of cell death[73]. Our results demonstrate that differential embryonic muscle contractions, which can be altered both genetically and epigenetically, may underlie the morphological diversification that has occurred during vertebrate evolution, including in vestigial structures such as the emu wing.

Methods

Data reporting
No statistical methods were used to predetermine the sample size. The experiments were not randomized, and the investigators were not blinded to allocation during the experiments and outcome assessment.

Animals
White Leghorn chicken (*Gallus gallus*) eggs were incubated at 37.5 °C and staged[74]. Fertilized emu (*Dromaius novaehollandiae*) eggs were purchased from Kakegawa Kachoen and Okhotsk Emu Pasture, incubated at 36 °C and staged as described in ref. 4. Wing samples of adult chickens were purchased post-mortem from a commercial supplier. Wing samples of adult emu were provided post-mortem from Tokyo Nodai Bioindustry Corporation. All animal work was performed in accordance with the guidelines for animal experiments of the Tokyo Institute of Technology, Kumamoto University, and The Jikei University School of Medicine, and the experimental protocols were approved by the committees of Tokyo Institute of Technology, and Kumamoto University. The sex of the animals was unknown.

Manipulation of embryo movement
Rigid paralysis[27] was induced in chicken embryos with decamethonium bromide (DMB), as previously described in ref. 29 with slight modifications. Briefly, embryos were immobilized between either E10-17 or E6-10. On the first day, 100 µl of sterile filtered 5 mg/ml DMB in 100 µl phosphate-buffered saline (PBS) was injected through the egg window onto the chorioallantoic membrane to induce immobilization. On each subsequent day, 100 µl of 1 mg/ml DMB in PBS was administered to maintain paralysis. Embryos were monitored by viewing through the egg window on each day of treatment and any DMB-treated embryos that were not fully paralyzed were excluded from the study. Control animals were administered only vehcle (PBS). The embryos were euthanized one day after the treatment and fixed in 4% paraformaldehyde. To quantify the rate of distal movements in the wings of embryos (Supplementary Fig. 1d), we recorded the behavior of stage 39 chicken and emu embryos incubated at 37.5 °C and 36 °C, respectively, through the window of the eggshell. Counts were conducted only when the embryos exhibited active movement, defined as any instance where the head, arms or legs were actively moving for more than 10 s. The rate of distal movements per individual was calculated as the distal movement count divided by the proximal movement count in five minutes of total active movement time. Proximal movement corresponded to extension and flexion of the elbow joint; distal movement corresponded to any wrist or phalangeal movement (Supplementary Fig. 2b).

Probe synthesis and in situ hybridization
Total RNA was extracted from stage 25–26 chickens, and stage 25 emu embryos using RNeasy kit (Qiagen). cDNA was synthesized by reverse transcription and used as a template for PCR. The construct used to synthesize RNA probes were based on the pBlueScript II SK(+), using In-Fusion HD Cloning Kits (Clontech). The primers used to amplify most of the gene fragments were designed with the forward (5′-ATC GATAAGCTTGAT...−3′) and reverse (5′-CTGCAGGAATTCGAT...−3′)

prefixes complementary to the ends of the linearized vector, which were followed by the specific sequences of the primers that were based on the indicated published sequences: chicken *Lbx1* (Ensembl, ENSGALG00000034189), 5′-CTGCGCTTCAACTTTTGCTC-3′ and 5′-GGTTCTGGAACCAGGTGAT-3′; chicken *MyoD* (GenBank accession number, NM_204214), 5′-CTTCTATGACGACCCGTGC-3′ and 5′-GTCTT GGAGCTTGGCTGAA-3′; emu *cMet* (Ensembl, ENSDNVG0000001 2888), 5′-AGGAGCCATGGACAATGCAA-3′ and 5′-CGAATGGACCTCTTC CTC-3′; emu *GlobinA* (Ensembl, ENSDNVT00000001340.1), 5′-GAG CTGCAACCATG-3′ and 5′-TGGCTGCTCGCTG-3′. For emu *Nkx2.5* (Ensembl, ENSDNVG00000013910.1), the open reading frame (ORF) of emu *Nkx2.5* was amplified using specific primers (5′-CCCACCG-CAATGTTTCCTAGCCCT-3′ and 5′-CTACCAGGCTCGGATCCCGTGCA-3′) and cloned into the *Eco*RV site of the pBlueScript SK(−) (pBSK-*Nkx2.5*). For emu *Lbx1* (Ensembl, ENSDNVG00000014711), emu genomic DNA was used as a template for PCR. The 5′ and 3′ fragments of emu *Lbx1* were amplified using the specific primers with the sequences complementary to the ends of the linearized pBlueScript II SK(+) (5′ fragment, 5′-ATCGATAAGCTTGATGTGGGCTTCAACTTTTGCTC-3′ and 5′-CTGCAGGAATTCGATGAGCCCCTTGAAGGTCTT-3′; 3′ fragment, 5′-ATCGATAAGCTTGATACCTATTCGTGGCCATGTCG-3′ and 5′-CTGC AGGAATTCGATCCGATGGGGCTGAGTGTAA-3′) and cloned into the vector using an In-Fusion HD Cloning Kit. The first exon sequence was obtained by fusing the DNA duplex synthesized using the oligonu-cleotides (5′-AGACCTTCAAGGGGCTCGAAGTGAGCGTGCTGCAGGCG GAATTCCTGCAGCCC-3′ and 5′-GGGCTGCAGGAATTCCGCCTGCAG-CACGCTCACTTCGAGCCCCTTGAAGGTCT-3′) into the *Hind*III site (3′ side) of the 5′ fragment. The full-length of emu *Lbx1* was obtained by cloning of the first exon sequence using specific primers with *Hind*III sequence (5′-GGTATCGATAAGCTTGATGTGGGCTTCAACTTTTG-3′ and 5′-GGAGACGCTGCGATTCGCCTGCAGCACGCT −3′), into the *Hin-d*III site of the vector including the second exon sequence, which was obtained by fusing the fragment amplified using the following primers by using In-Fusion HD Coning Kits (5′-GGTATCGATAAGCTTAAT CGCAGCGTCTCCCCTGC-3′ and 5′-CGACATGGCC ACGAATAGGT-3′) to the 5′ side of the 3′ fragment.

For in situ hybridization, embryos were fixed overnight in 4% paraformaldehyde in phosphate-buffered saline, dehydrated in a gra-ded methanol series and stored in 100% methanol at −20 °C. Whole-mount and section in situ hybridization were carried out as described[75,76]. For RNAscope in situ hybridization, probes for emu *cMet* (targeting 827–1801 bp of XM_026097341.1), emu *Nkx2.5* (targeting 2-1564 bp of XM_026122666.1), and emu *MyoD* (targeting 31–1358 bp of XM_026092794.1) were designed commercially by the manufacturer (Advanced Cell Diagnostics, Inc.). RNAscope in situ hybridization was performed using the RNAscope Fluorescent Multiplex Reagent Kit according to the manufacturer's instructions. HCR in situ hybridization was conducted according to the manufacturer's instructions. HCR probes targeting emu *Pax3* (XM_026109761.1) and *Hand2* (XM_026122869.1) were purchased commercially from Molecular Instruments, Inc. Images were obtained using an LSM 780 confocal microscope (Zeiss).

Histology
Whole-mount immunostaining was performed as previously described[77]. Supernatant containing the monoclonal anti-MYH1E anti-body was used to detect against myosin heavy chain (MF-20 hybri-doma clone, DSHB). Goat anti-mouse IgG, HRP-conjugated antibodies (HAF007, R&D Systems) were used at a concentration of 1:200. Section immunostaining was performed as described in ref. 78. Briefly, cryo-sections were incubated overnight with 1:1000 anti-cleaved caspase-8 antibody (9664, Cell signaling technology) or 1:100 anti-8-oxoguanine antibody (ab 64548, Abcam) at 4 °C. Sections were washed and incu-bated overnight with 1:1000 goat anti-rabbit IgG Alexa Fluor-488 conjugated antibody (ab150077, Abcam) or goat anti-mouse IgG Alexa

Fluor-488 conjugated antibody (Invitrogen) at 4 °C and then washed. For TUNEL staining, cryosections were stained using TUNEL Mix (In situ Cell Death Kit, Roche) according to the manufacturer's protocol. The sections were then incubated overnight with 1:400 sheep anti-fluorescein-AP antibody (Roche) at 4 °C and then washed. For Safranin-O staining, sections of embryos were prepared as described[79]. Briefly, embryos were fixed with 4% paraformaldehyde, dehydrated in ethanol and acetone, and embedded in Technovit 8100 resin (Heraues-Kulzer, Wehrheim, Germany). Sections were cut at a thickness of 8 μm and stained with Weigert's iron hematoxylin, Safranin-O and Fast Green as described in ref. 18. The narrowest parts of the interspace distance between the ulna and the distal carpus (chicken) or metacarpus (emu) were measured using cellSens software (Olympus).

Skeleton staining
Skeletons were stained according to standard protocols using Alcian blue for cartilage and Alizarin red for bone[80]. The length of individual bones was measured using Fiji[81].

Computed tomography imaging
Computed tomography (CT) imaging of adult emu forelimb skeletons was performed by a micro-CT system (Latheta LCT-200, Hitachi Aloka Medical Ltd., Tokyo, Japan). Acquired slice data were rendered as three-dimensional images using VGStudio MAX2.0 software (Volume Graphics GmbH., Heidelberg, Germany). Fusion of skeletal elements was evaluated by RadiAnt DICOM viewer (www.radiantviewer.com/).

Single-cell RNA sequencing and analysis
Trunk tissue at the forelimb level from four stage 20/21 emu embryos, and from fifteen forelimb buds from stage 25 emu embryos, were collected, pooled and then dissociated into single cells by enzymatic digestion as previously described[82], with modifications. Briefly, limb buds were treated with 2000 U dispase II (Wako) in Ca²⁺- and Mg²⁺-free Tyrode's solution (CMF-Tyrode) at 4 °C for 50 min and transferred to Dulbecco's modified Eagle's medium (DMEM) containing 1% fetal bovine serum (FBS), when their ectodermal sheets were removed by peeling off with a pair of forceps. Then, the remaining limb tissues or trunk tissues were transferred to Cellbanker 1 plus (Nippon Zenyaku Kogyo) and stored at −80 °C. Thawed tissues were washed in DMEM containing 0.04% bovine serum albumin (BSA), and incubated in CMF-Tyrode at 37 °C for 40 min. Softened tissues were dissociated into a single cell suspension by pipetting in DMEM containing 0.04% BSA. The suspension was first filtered using pluriStrainer-Mini 100 μm (pluriSelect), and the debris was removed using Debris Removal Solution (Miltenyi Biotec) according to the manufacturer's instruc-tions. Then, cells were filtered again using pluriStrainer-Mini 40 μm (pluriSelect), suspended in DMEM containing 2% BSA and proceeded immediately to cell encapsulation, indexing and transcriptome library prepration, as described below.

The single-cell transcriptome data of emu embryos were gener-ated at the Functional Genomics Facility of the National Institute for Basic Biology (NIBB) in Okazaki, Japan. For scRNAseq library con-struction, barcoded single-cell cDNA libraries were synthesized using 10x Genomics Chromium Single Cell 3′ Reagent Kits v3.1 (Dual Index) according to the manufacturer's instructions. Libraries were sequenced on an Illumina Hiseq platform at a depth of 117,418 and 48,543 mean reads per cell for stage 20/21 and stage 25 samples, respectively. The single-cell transcriptome data of chicken forelimbs were published previously[54]. Chicken forelimb single cell RNA sequence data of stage 24 (SRA accession numbers: SRR14570167 to SRR14570174) and stage 27 (SRA accession numbers: SRR14570175 to SRR14570178) were downloaded from the Sequence Read Archive (SRA).

Raw sequencing data were processedand aligned with a emu reference genome assembly droNov1 (GCF_003342905.1) or a chicken

reference genome assembly GRCg6a (Ensembl release 105) using Cell Ranger software version 7.1.0 (10x Genomics). Cell Ranger filtered outputs files for each dataset were processed using R package Seurat v4.3.0[83]. Following the standard pre-processing workflow of Seurat, low-quality cells and potential cell doublets were removed from the dataset. Gene expression was log normalized with NormalizedData and scaled with ScaleData using all genes. PCA-reduction was performed with RunPCA and nearest neighbor graph was constructed using the 50 PCs with FindNeighbors, and then clusters were identified using FindClusters. Cluster were assigned specific identities based on differentially expressed genes. To visualize these datasets, tSNE (t-distributed Stochastic Neighbor Embedding) was performed with RunTSNE using 1:50 dims as input. Differentially expressed genes for each cluster of emu and chicken data were provided by using the FindAllMarkers, which performs Wilcoxon rank-sum tests. Differential expression testing between *Pax3+/Hand2+* cells and *Pax3+/Hand2-* cells from the muscle cluster of stage 25 emu was conducted using the FindMakers function, which applies Wilcoxon rank-sum tests.

Statistical analysis

All statistical analyses, except for Figs. 3g and 5a, were performed with Prism 8.0.2 (GraphPad). *n* numbers represent the numbers of limbs, and measurements are represented as the mean ± SEM. All measurements were taken from distinct samples. Two-parameter comparisons between measurements of biological samples assumed unequal variances, thus Welch's unpaired *t*-test was used. The coefficient of variation was calculated as the ratio of the standard deviation to the mean. Statistical details can be found in the legends. Significance was defined at $P \leq 0.05$ (*$p < 0.05$, **$p < 0.01$, ***$p < 0.001$, ****$p < 0.0001$). For differentially expressed genes in Figs. 3g and 5a, the two-sided Wilcoxon rank-sum tests were used for statistical tests (*p*-val adjusted < 0.05).

Reporting summary

Further information on research design is available in the Nature Portfolio Reporting Summary linked to this article.

Data availability

The authors declare that all data supporting the findings of this study are available within the article and its Supplementary Information files. The raw sequencing data generated in this study have been deposited in the DDBJ Sequence Read Archive under accession numbers: DRA017391 and DRA014432; bioproject: PRJDB13845 and PRJDB16987. The publicly available chicken datasets, published before[54], were retrieved from Sequence Read Archive (SRA) under the accession numbers SRR14570167 to SRR14570174 (https://www.ncbi.nlm.nih.gov/sra/SRX10913414[accn]) and SRR14570175 to SRR14570178 (https://www.ncbi.nlm.nih.gov/sra/SRX10913415[accn]). Source data are provided with this paper.

Code availability

All code used to reproduce the Supplementary Fig. presented in this paper is publicly available through GiHub. The corresponding DOI is https://doi.org/10.5281/zenodo.11127881.

References

1. Xu, X. & Mackem, S. Tracing the evolution of avian wing digits. *Curr. Biol.* **23**, R538–R544 (2013).
2. Sackton, T. B. et al. Convergent regulatory evolution and loss of flight in paleognathous birds. *Science* **364**, 74–78 (2019).
3. Baker, A. J., Haddrath, O., McPherson, J. D. & Cloutier, A. Genomic support for a moa-tinamou clade and adaptive morphological convergence in flightless ratites. *Mol. Biol. Evol.* **31**, 1686–1696 (2014).
4. Nagai, H. et al. Embryonic development of the emu, Dromaius novaehollandiae. *Dev. Dyn.* **240**, 162–175 (2011).
5. de Bakker, M. A. et al. Digit loss in archosaur evolution and the interplay between selection and constraints. *Nature* **500**, 445–448 (2013).
6. Smith, C. A. et al. Limb patterning genes and heterochronic development of the emu wing bud. *Evodevo* **7**, 26 (2016).
7. Farlie, P. G. et al. Co-option of the cardiac transcription factor Nkx2.5 during development of the emu wing. *Nat. Commun.* **8**, 132 (2017).
8. Kawahata, K. et al. Evolution of the avian digital pattern. *Sci. Rep.* **9**, 8560 (2019).
9. Young, J. J., Grayson, P., Edwards, S. V. & Tabin, C. J. Attenuated Fgf Signaling Underlies the Forelimb Heterochrony in the Emu Dromaius novaehollandiae. *Curr. Biol.* **29**, 3681–3691.e3685 (2019).
10. Bickley, S. R. & Logan, M. P. Regulatory modulation of the T-box gene Tbx5 links development, evolution, and adaptation of the sternum. *Proc. Natl Acad. Sci. USA* **111**, 17917–17922 (2014).
11. Maxwell, E. E. & Larsson, H. C. Osteology and myology of the wing of the Emu (Dromaius novaehollandiae), and its bearing on the evolution of vestigial structures. *J. Morphol.* **268**, 423–441 (2007).
12. Nowlan, N. C., Sharpe, J., Roddy, K. A., Prendergast, P. J. & Murphy, P. Mechanobiology of embryonic skeletal development: Insights from animal models. *Birth Defects Res C. Embryo Today* **90**, 203–213 (2010).
13. Pitsillides, A. A. Early effects of embryonic movement: 'a shot out of the dark'. *J. Anat.* **208**, 417–431 (2006).
14. Felsenthal, N. & Zelzer, E. Mechanical regulation of musculoskeletal system development. *Development* **144**, 4271–4283 (2017).
15. Murphy, P. & Rolfe, R. A. Building a Co-ordinated Musculoskeletal System: The Plasticity of the Developing Skeleton in Response to Muscle Contractions. *Adv. Anat. Embryol. Cell Biol.* **236**, 81–110 (2023).
16. Rux, D., Decker, R. S., Koyama, E. & Pacifici, M. Joints in the appendicular skeleton: Developmental mechanisms and evolutionary influences. *Curr. Top. Dev. Biol.* **133**, 119–151 (2019).
17. Bamshad, M., Van Heest, A. E. & Pleasure, D. Arthrogryposis: a review and update. *J. Bone Jt. Surg. Am.* **91**, 40–46 (2009).
18. Nowlan, N. C. et al. Developing bones are differentially affected by compromised skeletal muscle formation. *Bone* **46**, 1275–1285 (2010).
19. Hamburger, V. & Balaban, M. Observations and experiments on spontaneous rhythmical behavior in the chick embryo. *Dev. Biol.* **7**, 533–545 (1963).
20. Bekoff, A. Embryonic development of chick motor behaviour. *Trends Neurosci.* **4**, 181–184 (1981).
21. Murray, P. D. F. An experimental study of the development of the limbs of the chick. *Proc. Linn. Soc. NSW* **51**, 179–263 (1926).
22. Fell, H. B. & Canti, R. G. Experiments on the development in vitro of the avian knee-joint. *Proc. R. Soc. Lond. Biol. Sci.* **116**, 316–351 (1934).
23. Pai, A. C. Developmental genetics of a Lethal Mutation, Muscular Dysgenesis (mdg) in the mouse. *Dev. Biol.* **11**, 82–92 (1965).
24. Drachman, D. B. & Sokoloff, L. The role of movement in embryonic joint development. *Dev. Biol.* **14**, 401–420 (1966).
25. Hall, B. K. & Herring, S. W. Paralysis and growth of the musculoskeletal system in the embryonic chick. *J. Morphol.* **206**, 45–56 (1990).
26. Mikic, B. et al. Differential effects of embryonic immobilization on the development of fibrocartilaginous skeletal elements. *J. Rehabil. Res Dev* **37**, 127–133 (2000).
27. Osborne, A. C., Lamb, K. J., Lewthwaite, J. C., Dowthwaite, G. P. & Pitsillides, A. A. Short-term rigid and flaccid paralyses diminish growth of embryonic chick limbs and abrogate joint cavity formation but differentially preserve pre-cavitated joints. *J. Musculoskelet. Neuronal Interact.* **2**, 448–456 (2002).

28. Lamb, K. J. et al. Diverse range of fixed positional deformities and bone growth restraint provoked by flaccid paralysis in embryonic chicks. *Int J. Exp. Pathol.* **84**, 191–199 (2003).

29. Pollard, A. S. et al. Limb proportions show developmental plasticity in response to embryo movement. *Sci. Rep.* **7**, 41926 (2017).

30. Nowlan, N. C., Prendergast, P. J. & Murphy, P. Identification of mechanosensitive genes during embryonic bone formation. *PLoS Comput. Biol.* **4**, e1000250 (2008).

31. Pollard, A. S., McGonnell, I. M. & Pitsillides, A. A. Mechanoadaptation of developing limbs: shaking a leg. *J. Anat.* **224**, 615–623 (2014).

32. Rolfe, R. A., Shea, C. A., Singh, P. N. P., Bandyopadhyay, A. & Murphy, P. Investigating the mechanistic basis of biomechanical input controlling skeletal development: exploring the interplay with Wnt signalling at the joint. *Philos. Trans. R. Soc. Lond. B Biol. Sci.* **373**, 20170329 (2018).

33. Alvares, L. E. et al. Intrinsic, Hox-dependent cues determine the fate of skeletal muscle precursors. *Dev. Cell* **5**, 379–390 (2003).

34. Jagla, K. et al. Mouse Lbx1 and human LBX1 define a novel mammalian homeobox gene family related to the Drosophila lady bird genes. *Mech. Dev.* **53**, 345–356 (1995).

35. Brohmann, H., Jagla, K. & Birchmeier, C. The role of Lbx1 in migration of muscle precursor cells. *Development* **127**, 437–445 (2000).

36. Gross, M. K. et al. Lbx1 is required for muscle precursor migration along a lateral pathway into the limb. *Development* **127**, 413–424 (2000).

37. Schafer, K. & Braun, T. Early specification of limb muscle precursor cells by the homeobox gene Lbx1h. *Nat. Genet* **23**, 213–216, (1999).

38. Okamoto, E. et al. Migratory appendicular muscles precursor cells in the common ancestor to all vertebrates. *Nat. Ecol. Evol.* **1**, 1731–1736 (2017).

39. Bladt, F., Riethmacher, D., Isenmann, S., Aguzzi, A. & Birchmeier, C. Essential role for the c-met receptor in the migration of myogenic precursor cells into the limb bud. *Nature* **376**, 768–771, (1995).

40. Dietrich, S. et al. The role of SF/HGF and c-Met in the development of skeletal muscle. *Development* **126**, 1621–1629 (1999).

41. Okamoto, E., Moriyama, Y., Kuraku, S., Kai, K. I. & Tanaka, M. Involvement of HGF/MET signaling in appendicular muscle development in cartilaginous fish. *Dev. Growth Differ.* **61**, 97–103 (2019).

42. Lyons, I. et al. Myogenic and morphogenetic defects in the heart tubes of murine embryos lacking the homeo box gene Nkx2-5. *Genes Dev.* **9**, 1654–1666 (1995).

43. Williams, B. A. & Ordahl, C. P. Pax-3 expression in segmental mesoderm marks early stages in myogenic cell specification. *Development* **120**, 785–796 (1994).

44. Srivastava, D., Cserjesi, P. & Olson, E. N. A subclass of bHLH proteins required for cardiac morphogenesis. *Science* **270**, 1995–1999 (1995).

45. Charite, J., McFadden, D. G. & Olson, E. N. The bHLH transcription factor dHAND controls Sonic hedgehog expression and establishment of the zone of polarizing activity during limb development. *Development* **127**, 2461–2470 (2000).

46. Yelon, D. et al. The bHLH transcription factor hand2 plays parallel roles in zebrafish heart and pectoral fin development. *Development* **127**, 2573–2582 (2000).

47. Onimaru, K., Shoguchi, E., Kuratani, S. & Tanaka, M. Development and evolution of the lateral plate mesoderm: comparative analysis of amphioxus and lamprey with implications for the acquisition of paired fins. *Dev. Biol.* **359**, 124–136 (2011).

48. Durland, J. L., Sferlazzo, M., Logan, M. & Burke, A. C. Visualizing the lateral somitic frontier in the Prx1Cre transgenic mouse. *J. Anat.* **212**, 590–602 (2008).

49. Bruneau, B. G. et al. Chamber-specific cardiac expression of Tbx5 and heart defects in Holt-Oram syndrome. *Dev. Biol.* **211**, 100–108 (1999).

50. Gibson-Brown, J. J., Agulnik, S. I., Silver, L. M., Niswander, L. & Papaioannou, V. E. Involvement of T-box genes Tbx2-Tbx5 in vertebrate limb specification and development. *Development* **125**, 2499–2509 (1998).

51. Logan, M., Simon, H. G. & Tabin, C. Differential regulation of T-box and homeobox transcription factors suggests roles in controlling chick limb-type identity. *Development* **125**, 2825–2835 (1998).

52. Isaac, A. et al. Tbx genes and limb identity in chick embryo development. *Development* **125**, 1867–1875 (1998).

53. Tanaka, M. Molecular and evolutionary basis of limb field specification and limb initiation. *Dev. Growth Differ.* **55**, 149–163 (2013).

54. Feregrino, C. & Tschopp, P. Assessing evolutionary and developmental transcriptome dynamics in homologous cell types. *Dev. Dyn.* **251**, 1472–1489 (2022).

55. Schwartz, L. M. Atrophy and programmed cell death of skeletal muscle. *Cell Death Differ.* **15**, 1163–1169 (2008).

56. Fernando, P., Kelly, J. F., Balazsi, K., Slack, R. S. & Megeney, L. A. Caspase 3 activity is required for skeletal muscle differentiation. *Proc. Natl Acad. Sci. USA* **99**, 11025–11030 (2002).

57. Dehkordi, M. H., Tashakor, A., O'Connell, E. & Fearnhead, H. O. Apoptosome-dependent myotube formation involves activation of caspase-3 in differentiating myoblasts. *Cell Death Dis.* **11**, 308 (2020).

58. Aram, L. et al. A Krebs Cycle Component Limits Caspase Activation Rate through Mitochondrial Surface Restriction of CRL Activation. *Dev. Cell* **37**, 15–33 (2016).

59. Schoenmann, Z. et al. Axonal degeneration is regulated by the apoptotic machinery or a NAD+-sensitive pathway in insects and mammals. *J. Neurosci.* **30**, 6375–6386 (2010).

60. Akbari-Birgani, S., Hosseinkhani, S., Mollamohamadi, S. & Baharvand, H. Delay in apoptosome formation attenuates apoptosis in mouse embryonic stem cell differentiation. *J. Biol. Chem.* **289**, 16905–16913 (2014).

61. Zuniga, A., Haramis, A. P., McMahon, A. P. & Zeller, R. Signal relay by BMP antagonism controls the SHH/FGF4 feedback loop in vertebrate limb buds. *Nature* **401**, 598–602 (1999).

62. Scherz, P. J., Harfe, B. D., McMahon, A. P. & Tabin, C. J. The limb bud Shh-Fgf feedback loop is terminated by expansion of former ZPA cells. *Science* **305**, 396–399 (2004).

63. Verheyden, J. M. & Sun, X. An Fgf/Gremlin inhibitory feedback loop triggers termination of limb bud outgrowth. *Nature* **454**, 638–641 (2008).

64. Zeller, R. The temporal dynamics of vertebrate limb development, teratogenesis and evolution. *Curr. Opin. Genet Dev.* **20**, 384–390 (2010).

65. Lopez-Rios, J. et al. GLI3 constrains digit number by controlling both progenitor proliferation and BMP-dependent exit to chondrogenesis. *Dev. Cell* **22**, 837–848 (2012).

66. Liu, P. et al. Effects of Mechanical Stress Stimulation on Function and Expression Mechanism of Osteoblasts. *Front Bioeng. Biotechnol.* **10**, 830722 (2022).

67. Deng, Y. et al. Yap1 Regulates Multiple Steps of Chondrocyte Differentiation during Skeletal Development and Bone Repair. *Cell Rep.* **14**, 2224–2237 (2016).

68. Rolfe, R. A. et al. Identification of mechanosensitive genes during skeletal development: alteration of genes associated with cytoskeletal rearrangement and cell signalling pathways. *BMC Genomics* **15**, 48 (2014).

69. Esteves de Lima, J., Bonnin, M. A., Birchmeier, C. & Duprez, D. Muscle contraction is required to maintain the pool of muscle progenitors via YAP and NOTCH during fetal myogenesis. *Elife* **5**, e15593 (2016).

70. Flynn, C. G. K. et al. Hox11-expressing interstitial cells contribute to adult skeletal muscle at homeostasis. *Development* **150**, dev201026 (2023).

71. Yaseen, W. et al. Fibroblast fusion to the muscle fiber regulates myotendinous junction formation. *Nat. Commun.* **12**, 3852 (2021).

72. West-Eberhard, M. J. Phenotypic accommodation: adaptive innovation due to developmental plasticity. *J. Exp. Zool. B Mol. Dev. Evol.* **304**, 610–618 (2005).

73. Tran, M. P. et al. Evolutionary loss of foot muscle during development with characteristics of atrophy and no evidence of cell death. *Elife* **8**, e50645 (2019).

74. Hamburger, V. & Hamilton, H. A series of normal stages in the development of the chick embryo. *J. Morph.* **88**, 49–92 (1951).

75. Wilkinson, D. G. In Situ Hybridization: A Practical Approach. (Oxford University Press, 1992).

76. Yoshida, N., Urase, K., Takahashi, J., Ishii, Y. & Yasugi, S. Mucus-associated antigen in epithelial cells of the chicken digestive tract: Developmental change in expression and implications for morphogenesis-function relationships. *Dev. Growth Differ.* **38**, 185–192 (1996).

77. Horigome, N. et al. Development of cephalic neural crest cells in embryos of Lampetra japonica, with special reference to the evolution of the jaw. *Dev. Biol.* **207**, 287–308 (1999).

78. Cordeiro, I. R. et al. Environmental Oxygen Exposure Allows for the Evolution of Interdigital Cell Death in Limb Patterning. *Dev. Cell* **50**, 155–166.e154 (2019).

79. Kaneko, H., Nakatani, Y., Fujimura, K. & Tanaka, M. Development of the lateral plate mesoderm in medaka Oryzias latipes and Nile tilapia Oreochromis niloticus: Insight into the diversification of pelvic fin position. *J. Anat.* **225**, 659–674 (2014).

80. Ojeda, J. L., Barbosa, E. & Bosque, P. G. Selective skeletal staining in whole chicken embryos; a rapid Alcian blue technique. *Stain Technol.* **45**, 137–138 (1970).

81. Schindelin, J. et al. Fiji: an open-source platform for biological-image analysis. *Nat. Methods* **9**, 676–682 (2012).

82. Wada, N., Tanaka, H., Ide, H. & Nohno, T. Ephrin-A2 regulates position-specific cell affinity and is involved in cartilage morphogenesis in the chick limb bud. *Dev. Biol.* **264**, 550–563 (2003).

83. Hao, Y. et al. Integrated analysis of multimodal single-cell data. *Cell* **184**, 3573–3587.e3529 (2021).

Author contributions

E.T., I.R.C., S.F.O. and M.T. designed the project and wrote the manuscript. E.T. analyzed the length and patterns of skeletal elements and muscles, I.R.C. examined gene expression, S.F.O. examined the movement of embryos, and performed scRNA-seq analyses, S.F.O. and T.K. captured confocal images, M.T. performed histology, immunology and examined gene expression by using DIG-, RNA scope- and HCR-probes, R.Y. constructed plasmids, S.S. provided sequencing research infrastructures, G.S. provided plasmids related to blood differentiation and emu embryos. M.K. took CT images, M.O. assisted with CT scanning.

Competing interests

The authors declare no competing interests.

Additional information

Supplementary information The online version contains supplementary material available at https://doi.org/10.1038/s41467-024-52203-x.

Correspondence and requests for materials should be addressed to Mikiko Tanaka.

Peer review information *Nature Communications* thanks Sevan Hopyan and the other, anonymous, reviewer(s) for their contribution to the peer review of this work. A peer review file is available.

Reprints and permissions information is available at http://www.nature.com/reprints

Publisher's note Springer Nature remains neutral with regard to jurisdictional claims in published maps and institutional affiliations.